Formulation of the rotational transformation of wave fields and their application to digital holography

Kyoji Matsushima

Department of Electrical and Electronic Engineering, Kansai University,
Yamate-cho 3-3-35, Suita, Osaka 564-8680, Japan

*Corresponding author: matsu@kansai-u.ac.jp

Rotational transformation based on coordinate rotation in Fourier space is a useful technique for simulating wave field propagation between nonparallel planes. This technique is characterized by fast computation because the transformation only requires executing a fast Fourier transform twice and a single interpolation. It is proved that the formula of the rotational transformation mathematically satisfies the Helmholtz equation. Moreover, to verify the formulation and its usefulness in wave optics, it is also demonstrated that the transformation makes it possible to reconstruct an image on arbitrarily tilted planes from a wave field captured experimentally by using digital holography.   © 2008 Optical Society of America

OCIS codes: 090.1995, 350.5500, 000.3860.

1. Introduction

Simulation in wave optics has become increasingly more important because of the evolution of modern optical technologies such as diffractive optical elements and digital holography. In these technologies, exact and fast simulation techniques are always demanded, especially for free space propagation. There are various formulations for spatial propagation or diffraction of coherent wave fields in a free space, including such well-known formulas as the Fresnel–Kirchhoff integral or Fresnel and Fraunhofer diffraction. However, these share a common restriction: the reference screen must be parallel to the source plane in which the wave field is initially given. Formulations based on coordinate rotation in Fourier space [1,2] and the Rayleigh–Sommerfeld integral [3] have been presented for removing this restriction. A similar formulation based on the Fresnel approximation is also reported for numerical reconstruction in digital holography [4].

Recently, the author and colleagues presented another formulation for propagation between nonparal-

lel planes [5]. This formula, referred to as rotational transformation, features exact and fast simulation. Since this is a useful technique, applications using the presented formula have been reported for creating surface objects [6] and hidden-surface removal [7] in computer-generated holograms and for the numerical reconstruction of digital holograms [8]. However, slight doubts regarding the mathematical reliability of the formula have not been dispelled, because the derivation in [5] is based on the physical interpretation of the angular spectrum of plane waves.

I aim to provide a brief proof that the formula rigorously satisfies the Helmholtz equation and that there are no approximations included in the formulation. Another aim is to demonstrate the application of rotational transformation to digital holography. Evolution of computer technology is realizing various possibilities for digital signal processing of light. Digital signal processing makes it possible to process light wave fields in a manner that is difficult or impossible to accomplish by using conventional optical components. Digital holography is a critical technology for acquisition of wave fields in digital signal processing of light. For example, De Nicola *et al.* used digital holography and reported correct image recon-

struction under conditions of severe anamorphism [9]. They also reported numerical reconstruction of images on tilted planes [8] using digital holography and rotational transformation based on the formulation presented in an earlier paper of ours [5]. However, the results reported by De Nicola *et al.* are of holographic microscopy for an object with dimensions of several micrometers. In this paper, reconstruction of a large object with dimensions of $4 \, \text{cm} \times 1 \, \text{cm}$ is demonstrated for experimental verification of rotational transformation.

2. Formulation of Rotational Transformation

A. Coordinate Systems and Rotation Matrices

Two coordinate systems are defined as shown in Fig. 1. One of the coordinate sets is referred to as the source coordinate (x, y, z). A wave field is initially given in the plane $(x, y, 0)$ of the source coordinates. This plane is referred to as the source plane. The reference coordinates $(\hat{x}, \hat{y}, \hat{z})$ are the second set of coordinates, in which a wave field is calculated by rotational transformation in the plane $(\hat{x}, \hat{y}, 0)$, referred to as the reference plane. Both coordinate systems share the origin and are not parallel to each other.

Position vectors $\mathbf{r} = (x, y, z)$ and $\hat{\mathbf{r}} = (\hat{x}, \hat{y}, \hat{z})$ can be mutually transformed by the transformation matrix $\mathbf{T}$ as follows:

$$\hat{\mathbf{r}} = \mathbf{T}\mathbf{r}, \tag{1}$$

$$\mathbf{r} = \mathbf{T}^{-1}\hat{\mathbf{r}}. \tag{2}$$

The matrix $\mathbf{T}$ is, in general, given as a rotation matrix $\mathbf{R}_\xi(\theta_\xi)$ or the product of several rotation matrices as follows:

$$\mathbf{T} = \mathbf{R}_\xi(\theta_\xi)...\mathbf{R}_\eta(\theta_\eta), \tag{3}$$

where ξ and η denote axes x, y, or z and θ_ξ and θ_η are the angles of rotation around the axes ξ and η, respectively. Individual rotation matrices are shown in Table 1. These commonly possess the following characteristics:

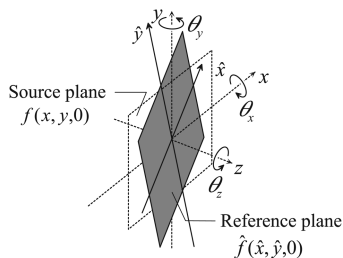$$\mathbf{R}_\xi^{-1}(\theta_\xi) = \mathbf{R}_\xi(-\theta_\xi) = {}^t\mathbf{R}_\xi(\theta_\xi), \tag{4}$$

Fig. 1. Definition of the coordinate systems and their rotation.

where $\mathbf{R}_\xi^{-1}(\theta_\xi)$ and ${}^t\mathbf{R}_\xi(\theta_\xi)$ are the inverse and transposed matrix of a rotation matrix, respectively.

As a result, the inverse matrix of any transformation matrix defined by the product of individual rotation matrices in Eq. (3) is generally given by

$$\mathbf{T}^{-1} = {}^t\mathbf{T}. \tag{5}$$

Therefore, the generalized transformation matrix below is used in formulations as follows:

$$\mathbf{T}^{-1} = \begin{bmatrix} a_1 & a_2 & a_3 \\ a_4 & a_5 & a_6 \\ a_7 & a_8 & a_9 \end{bmatrix}, \tag{6}$$

$$\mathbf{T} = \begin{bmatrix} a_1 & a_4 & a_7 \\ a_2 & a_5 & a_8 \\ a_3 & a_6 & a_9 \end{bmatrix}. \tag{7}$$

B. Rotational Transformation

When a wave field $f(x, y, 0)$ with wavelength λ is given in the source plane, the source field at arbitrary positions is given by [10]

$$\begin{aligned} f(x, y, z) &= \int \int_{-\infty}^{+\infty} F(u, v) \exp[i2\pi\{ux + vy \\ &\quad + (\lambda^{-2} - u^2 - v^2)^{1/2}z\}]\mathrm{d}u\mathrm{d}v \\ &= \mathcal{F}^{-1}\{F(u, v) \exp[i2\pi w(u, v)z\}, \end{aligned} \tag{8}$$

$$w(u, v) = (\lambda^{-2} - u^2 - v^2)^{1/2}, \tag{9}$$

where $F(u, v)$ and $[u, v, w(u, v)]$ are the Fourier spectrum of $f(x, y, 0)$ and Fourier frequencies for (x, y, z), respectively. Note that the wave field $f(x, y, z)$ represented in Eq. (8) rigorously satisfies the Helmholtz equation.

The wave field in the reference plane $\hat{f}(\hat{x}, \hat{y}, \hat{z} = 0)$ is given by substituting Eq. (2) and $\mathbf{T}^{-1}$ of Eq. (6) into Eq. (8) as follows:

$$\begin{aligned} \hat{f}(\hat{x}, \hat{y}, 0) &= f(a_1\hat{x} + a_2\hat{y}, a_4\hat{x} + a_5\hat{y}, a_7\hat{x} + a_8\hat{y}) \\ &= \int \int F(u, v) \exp[\{i2\pi[(a_1u + a_4v + a_7w)\hat{x} \\ &\quad + (a_2u + a_5v + a_8w)\hat{y}]\}]\mathrm{d}u\mathrm{d}v, \end{aligned} \tag{10}$$

where the abbreviation $w = w(u, v)$ is used.

When Fourier frequencies $\hat{u}$, $\hat{v}$, and $\hat{w} = \hat{w}(\hat{u}, \hat{v}) = (\lambda^{-2} - \hat{u}^2 - \hat{v}^2)^{1/2}$ are defined with respect to $\hat{x}$, $\hat{y}$, and $\hat{z}$, the vectors $\mathbf{f} = (u, v, w)$ and $\hat{\mathbf{f}} = (\hat{u}, \hat{v}, \hat{w})$ in the Fourier space are transformed into each other by the same transformation matrices $\mathbf{T}$ and $\mathbf{T}^{-1}$ as in real space. Therefore, by using the transform $\hat{\mathbf{f}} = \mathbf{T}\mathbf{f}$, the exponent in Eq. (10) can be reduced to $i2\pi(\hat{u}\hat{x} + \hat{v}\hat{y})$, and the wave field in the reference

Table 1. Rotation Matrices

$$\mathbf{R}_x(\theta_x) = \begin{pmatrix} 1 & 0 & 0 \\ 0 & \cos\theta_x & \sin\theta_x \\ 0 & -\sin\theta_x & \cos\theta_x \end{pmatrix}, \qquad \mathbf{R}_y(\theta_y) = \begin{pmatrix} \cos\theta_y & 0 & -\sin\theta_y \\ 0 & 1 & 0 \\ \sin\theta_y & 0 & \cos\theta_y \end{pmatrix}, \qquad \mathbf{R}_z(\theta_z) = \begin{pmatrix} \cos\theta_z & \sin\theta_z & 0 \\ -\sin\theta_z & \cos\theta_z & 0 \\ 0 & 0 & 1 \end{pmatrix}$$

plane is given as

$$\hat{f}(\hat{x},\hat{y},0) = \int\int F(\alpha(\hat{u},\hat{v}),\beta(\hat{u},\hat{v}))$$
$$\times \exp[i2\pi(\hat{u}\hat{x}+\hat{v}\hat{y})]\mathrm{d}u\mathrm{d}v, \qquad (11)$$

where arguments u and v of spectrum $F(u,v)$ in Eq. (10) are rewritten by using $\mathbf{f} = \mathbf{T}^{-1}\hat{\mathbf{f}}$ as follows:

$$u = \alpha(\hat{u},\hat{v}) \equiv a_1\hat{u} + a_2\hat{v} + a_3\hat{w}(\hat{u},\hat{v}),$$
$$v = \beta(\hat{u},\hat{v}) \equiv a_4\hat{u} + a_5\hat{v} + a_6\hat{w}(\hat{u},\hat{v}). \qquad (12)$$

Changing from variables u, v to $\hat{u}, \hat{v}$ in the integration of Eq. (11) can be achieved by substituting $\mathrm{d}u\mathrm{d}v = |J(\hat{u},\hat{v})|\mathrm{d}\hat{u}\mathrm{d}\hat{v}$ and the Jacobian obtained by

$$J(\hat{u},\hat{v}) = \frac{\partial\alpha}{\partial\hat{u}}\frac{\partial\beta}{\partial\hat{v}} - \frac{\partial\alpha}{\partial\hat{v}}\frac{\partial\beta}{\partial\hat{u}}. \qquad (13)$$

As a result, rotational transformation of the wave fields is formulated as follows:

$$\hat{f}(\hat{x},\hat{y},0) = \int\int \hat{F}(\hat{u},\hat{v})\exp[i2\pi(\hat{u}\hat{x}+\hat{v}\hat{y})]\mathrm{d}\hat{u}\mathrm{d}\hat{v}$$
$$= \mathcal{F}^{-1}\{\hat{F}(\hat{u},\hat{v})\}, \qquad (14)$$

$$\hat{F}(\hat{u},\hat{v}) = F(a_1\hat{u} + a_2\hat{v} + a_3\hat{w}(\hat{u},\hat{v}), a_4\hat{u} + a_5\hat{v} + a_6\hat{w}(\hat{u},\hat{v}))|J(\hat{u},\hat{v})|, \qquad (15)$$

$$J(\hat{u},\hat{v}) = \frac{(a_2a_6 - a_3a_5)\hat{u}}{\hat{w}(\hat{u},\hat{v})} + \frac{(a_3a_4 - a_1a_6)\hat{v}}{\hat{w}(\hat{u},\hat{v})} + (a_1a_5 - a_2a_4). \qquad (16)$$

The Jacobian approximates a constant and therefore can be ignored in cases where the field is paraxial in the source or reference coordinates [5]. It is worth emphasizing that $\hat{f}(\hat{x},\hat{y},0)$ given by Eqs. (14)–(16) is a complete solution of the Helmholtz equation. In addition, only a double Fourier transform is needed to perform this transformation.

C. Resampling Fourier Spectrum

Since fast Fourier transforms (FFTs) are commonly used for numerical calculation, the source spectrum $F(u,v)$ is sampled in a square area, and the center of the sampling area is the origin of the Fourier space, as shown in Fig. 2(a). However, as shown in 2(b), the

origin in the source Fourier space (u,v) is projected to $(\hat{u}_0,\hat{v}_0) = (a_7\lambda^{-1}, a_8\lambda^{-1})$ in the reference Fourier space by the transform $\hat{\mathbf{f}} = \mathbf{T}\mathbf{f}$. Therefore, the second FFT required in Eq. (14) does not work effectively because the spectrum is sampled far from the origin. To use FFTs for numerical calculation, shifted Fourier space $(\tilde{u},\tilde{v}) = (\hat{u} - \hat{u}_0, \hat{v} - \hat{v}_0)$ should be introduced in order to cancel these undesired offsets. When using these shifted Fourier frequencies, the spectrum in the reference plane is rewritten as

$$\hat{F}(\hat{u},\hat{v}) = \hat{F}(\tilde{u}+\hat{u}_0, \tilde{v}+\hat{v}_0) = \tilde{F}(\tilde{u},\tilde{v}). \qquad (17)$$

An example of a sampling area in the shifted reference space is shown in Fig. 2(c).

Let us invert the procedure. Suppose that the spectrum $\tilde{F}(\tilde{u},\tilde{v})$ is sampled in a square area centered in the shifted Fourier space, as shown in Fig. 2(f), the origin of $(\tilde{u},\tilde{v})$ agrees with the center of the spectrum $(\hat{u},\hat{v}) = (\hat{u}_0,\hat{v}_0)$ in the reference Fourier space, as shown in 2(e), and the origin in the source Fourier space, in 2(d). The sampling point $(\tilde{u},\tilde{v})$ is projected to the source Fourier space (u,v) as follows:

$$u = \alpha(\tilde{u}+\hat{u}_0, \tilde{v}+\hat{v}_0), \qquad (18)$$
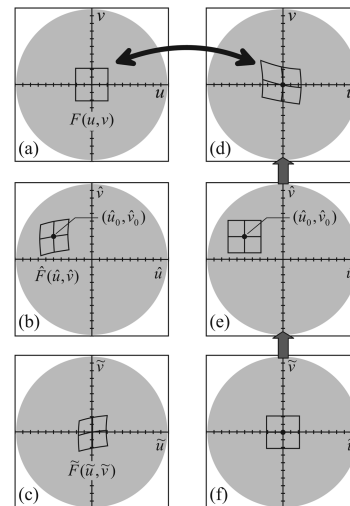

Fig. 2. Example of sampling areas in three Fourier spaces: (a), (d) source, (b), (e) reference, and (c), (f) shifted reference Fourier spaces. The left-hand column (a)–(c) is the case of a spectrum sampled in an equidistant grid within the square area in the source space, whereas the right-hand column (d)–(f) is for equidistant and square sampling in a shifted reference space. This example is for $\mathbf{T} = \mathbf{R}_x(20°)\mathbf{R}_y(30°)$.

$$v = \beta(\tilde{u} + \hat{u}_0, \tilde{v} + \hat{v}_0). \qquad (19)$$

When both $\tilde{F}(\tilde{u}, \tilde{v})$ and $F(u, v)$ are sampled in equidistant sampling grids, the sampling points in the sampled spectrum $F(u, v)$ generally do not agree with the sampling points in $\tilde{F}(\tilde{u}, \tilde{v})$ because of the distortion of the sampling grid caused by the projection in Eqs. (18) and (19). As a result, an interpolation is necessary for resampling $\tilde{F}(\tilde{u}, \tilde{v})$ from $F(u, v)$.

The inverse Fourier transform of Eq. (17) as to $\tilde{u}, \tilde{v}$ is given by using the shift theorem as

$$\begin{aligned} \mathcal{F}^{-1}\{\tilde{F}(\tilde{u}, \tilde{v})\} &= \mathcal{F}^{-1}\{\hat{F}(\tilde{u} + \hat{u}_0, \tilde{v} + \hat{v}_0)\} \\ &= \mathcal{F}^{-1}\{\hat{F}(\tilde{u}, \tilde{v})\} \exp[-i2\pi(\hat{u}_0\hat{x} + \hat{v}_0\hat{y})]. \end{aligned} \qquad (20)$$

Since the inverse Fourier transform of $\hat{F}(\hat{u}, \hat{v})$ as to $\hat{u}, \hat{v}$ is identical to that of $\hat{F}(\tilde{u}, \tilde{v})$ as to $\tilde{u}, \tilde{v}$, we can rewrite Eq. (14) as

$$\hat{f}(\hat{x}, \hat{y}, 0) = \mathcal{F}^{-1}\{\tilde{F}(\tilde{u}, \tilde{v})\} \exp[i2\pi(\hat{u}_0\hat{x} + \hat{v}_0\hat{y})]. \qquad (21)$$

In the case of a slight tilting of the source plane, the Fourier spectrum in the reference plane can be approximated to the source one, i.e., $\tilde{F}(\tilde{u}, \tilde{v}) \approx F(u, v)$; therefore, $\hat{f}(\hat{x}, \hat{y}, 0) \approx f(x, y, 0) \exp[i2\pi(\hat{u}_0\hat{x} + \hat{v}_0\hat{y})]$ is a good approximation. This agrees with the theoretical method providing analysis of the effect of the slight tilting motion of object surfaces [11].

In summary, the spectrum $F(u, v)$ of the source wave field is first calculated by using a FFT in the numerical implementation of the theory presented here. Next, the spectrum $\tilde{F}(\tilde{u}, \tilde{v})$ is resampled from $F(u, v)$ by using an interpolation as follows:

$$\begin{aligned} \tilde{F}(\tilde{u}, \tilde{v}) &\cong F(\alpha(\tilde{u} + \hat{u}_0, \tilde{v} + \hat{v}_0), \beta(\tilde{u} + \hat{u}_0, \tilde{v} + \hat{v}_0)) \\ &\quad |J(\tilde{u} + \hat{u}_0, \tilde{v} + \hat{v}_0)|. \end{aligned} \qquad (22)$$

Finally, the wave field in the reference coordinates is obtained by inverse FFT in Eq. (21).

3. Application of Rotational Transformation to Digital Holography

To verify the above formulation of the rotational transformation, an attempt to reconstruct clear images of the pattern printed on a tilted plane was performed by using digital holography. As shown in Fig. 3, the wave field emitted from the planar object, on which some letters are printed, was captured on the image sensor by using phase-shifting digital holography. The printed pattern (letters) covering an area of 4 cm × 1 cm is shown in Fig. 4.

A. Experimental Setup

The wave field from the tilted planar object was captured by using the aliasing-free zone [12] in phase-shifting lensless Fourier digital holography. This is because the object is large compared with those used in holographic microscopy [8]. The aliasing-free zone
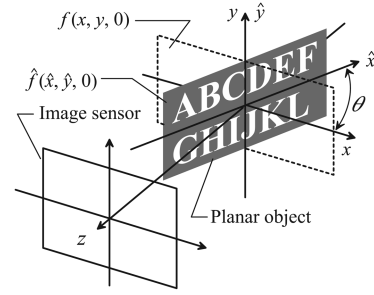

Fig. 3. Schematics for capturing the wave field from a tilted plane.

is a virtual zone in the shape of a quadrangular pyramid in the object space, as shown in Fig. 5. An object wave emitted from any object placed within the zone can be recorded without any aliasing error. The shape of the aliasing-free zone is obtained from an estimation of the maximum spatial frequency on the sensor surface and is presented as the relationship between the object width w and the object distance d from the image sensor, as follows [12]:

$$w \le \frac{4\lambda d}{\sqrt{16\delta^2 - \lambda^2}}, \qquad (23)$$

where δ is the sensor pitch. We can minimize the object distance and maximize the object size by using the aliasing-free zone. As a result, the angle of the visual field can be maximized to the limit imposed by the sensor pitch.

The experimental setup for capturing the wave field by the phase-shifting lensless Fourier digital holography is shown in Fig 6. The planar object illuminated with coherent light ($\lambda = 532\,\text{nm}$) is slanted at approximately 70° around the y axis, and the distance between the center of the object and the image sensor is approximately 19.5 cm. The piezo phase shifter is inserted into the reference path to change the phase of the reference field. Furthermore, the spatial filter forms the reference field into a spherical wave. A CMOS-type high-resolution image sensor with sensor pitches of $6.0\,\mu\text{m} \times 6.0\,\mu\text{m}$ is used to capture the fringe pattern. The number of pixels of the image sensor is 2000 × 2000 pixels.

B. Numerical Reconstruction by Rotational Transformation

A schematic procedure for reconstructing a pattern on a tilted planar object is shown in Fig. 7. The complex image $g(x_0, y_0)$ was composed from four different
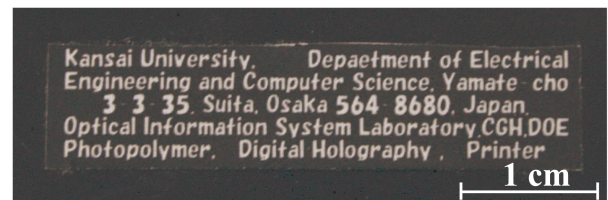

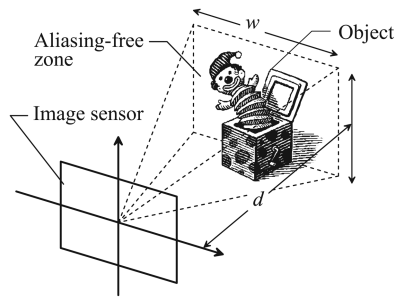Fig. 4. (Color online) Photograph of the pattern printed on the planar object.

Fig. 5. Schematic illustration of an aliasing-free zone.

phase-shifting fringe patterns captured by the image sensor [13]. The wave field $f'(x,y,z'=-z_R)$ was obtained in the plane parallel to the image sensor by using a Fourier transform as follows:

$$f'(x,y,z'=-z_R) = \mathcal{F}\{g(x_0,y_0)\}_{u=-x/\lambda z_R, v=-y/\lambda z_R}, \quad (24)$$

where the origin of z' is on the sensor surface and z_R is the distance between the sensor surface and the pinhole of the spatial filter inserted into the reference path, as shown in Fig. 6.

A close-up photograph of the tilted planar object captured by an ordinary lens camera is shown in Fig. 8(a). Similar images can be obtained as the amplitude image $|f'(x,y,-z_R)|$, as shown in Fig. 8(b). In this amplitude image, the number of samplings and sampling pitches have changed from that of the image sensor because of the Fourier transform in Eq. (24). These are 2048 × 2048 pixels and 8.1 μm × 8.1 μm in Fig. 8(b), respectively.

We cannot obtain clear images in both results in Fig. 8 because of the depth of focus. Rotational transformation should be used to produce a clear image on the surface of the planar object. However, if the center of the sampled wave field $f'(x,y,-z_R)$ does not coincide with the surface of the planar object exactly, we cannot obtain a clear image, because rotational transformation yields the wave field rotated on the center of the sampling area. Therefore, the field $f'(x,y,-z_R)$ must be propagated to the position $z'=-z_R-\Delta z$ numerically so that the center of the field is exactly placed on the surface of the planar object,
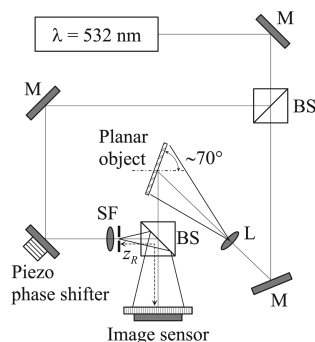

Fig. 6. Experimental setup for recording phase-shifting lensless Fourier digital holograms: L, lens; M, mirror; BS, beam splitter; SF, spatial filter.
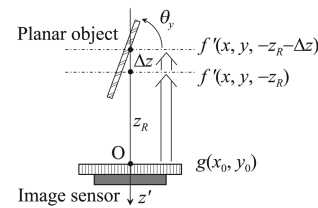

Fig. 7. Procedure for numerical reconstruction of images on the planar object from the complex image captured on the image sensor.

as shown in Fig. 7. We can use any method for this propagation. In this paper, the angular spectrum of the plane wave in Eq. (8) is used for this numerical propagation.

The wave field $f'(x,y,-z_R-\Delta z)$ is the starting point of rotational transformation, i.e., $f(x,y,0) = f'(x,y,-z_R-\Delta z)$, and transformation matrix $\mathbf{T} = \mathbf{R}_y(\theta_y)$ was used in the calculation. First, the spectrum $F(u,v)$ is calculated by using an FFT. Next, the spectrum in the shifted reference Fourier space $\tilde{F}(\tilde{u},\tilde{v})$ is obtained by resampling $F(u,v)$, using Eq. (22). Since the complex value of the spectrum $F[\alpha(\tilde{u}_m+\hat{u}_0,\tilde{v}_n+\hat{v}_0),\beta(\tilde{u}_m+\hat{u}_0,\tilde{v}_n+\hat{v}_0)]$ must be obtained for each sampling point $(\tilde{u}_m,\tilde{v}_n)$ on the equidistant sampling grid, interpolation is needed because of the nonlinearity attributed to Eq. (12).

Finally, we can calculate the wave field in the reference plane by use of Eq. (21). Since the purpose of this experiment is to calculate only the amplitude image, the phase factor in Eq. (21) can be ignored; i.e., the FFT is performed only in $\tilde{F}(\tilde{u},\tilde{v})$. The amplitude image $|\hat{f}(\hat{x},\hat{y},0)|$ after the rotational transformation at $\theta_y = 71.8°$ is shown in Fig. 9. The whole pattern on the surface of the tilted planar object appears clearly when compared with the results in Fig. 8.

The case of two-axis rotation is shown in Fig. 10. The planar object is slanted at 30° around the y axis after rotation at −60° around the x axis. Therefore the transformation matrix $\mathbf{T} = \mathbf{R}_y(30°)\mathbf{R}_x(-60°)$ is used to retrieve the original pattern.

4. Discussion

In this paper rotational transformation is used to retrieve the original pattern printed on tilted planes. In some cases, however, the inverse problem could be more interesting. Figure 11 shows the case of tilting the image sensor; i.e., the sensor surface is not perpendicular to the normal line of the object surface. Even in this case, distortion of the captured field is most likely compensated by the rotational trans-
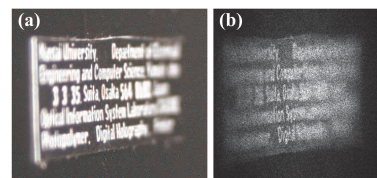

Fig. 8. (Color online) (a) Close-up photograph of the object and (b) the amplitude image $|f'(x,y,-z_R)|$ numerically reconstructed in the plane parallel to the image sensor.
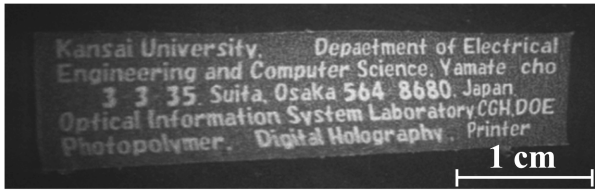
Fig. 9. Amplitude image of the wave field calculated in the tilted plane by rotational transformation.

Fig. 11. Procedure for compensation for tilting a sensor surface by rotational transformation.

Fig. 12. (Color online) Tomographic imaging of a transparent specimen by rotational transformation. P_n and S_n are planes parallel and nonparallel to the image sensor, respectively.

formation. The sequence of the numerical reconstruction is, however, different from the object rotation shown in Fig. 7. Assuming that the wave field $f(x, y, 0)$ on the sensor surface is captured by some type of digital holography, the wave field must be rotationally transformed prior to translational propagation. Once the field $\hat{f}(\hat{x}, \hat{y}, 0)$ is obtained in a plane parallel to the object surface, the wave field $\hat{f}(\hat{x}, \hat{y}, -\Delta z)$ can be reconstructed by using ordinary digital holography methods.

Reconstruction of the surface pattern of a slanted opaque object is adopted for experimental verification of the rotational transformation formulated in this paper. However, numerical reconstruction of transparent objects by using rotational transformation may be interesting for some biological applications. A conceptual illustration in such a case is shown in Fig. 12. When the object wave of a specimen with sparse contents or a slight change of refractive index is captured by digital holography, we can reconstruct tomographic images in planes parallel to the sensor by ordinary techniques. Rotational transformation makes it possible to reconstruct tomographic images in any plane in the object space. The reconstruction plane is no longer limited to the parallel ones. As well, the computational complexity of the rotational transformation is only a double FFT and an interpolation. Therefore, computation time is almost the same as that for reconstruction in a parallel plane.

5. Conclusion

In conclusion, I proved that the rotational transformation formula presented in [5] satisfies the Helmholtz equation and therefore gives an exact spatial solution of the wave equation. This rotational transformation has the advantage of easy implementation and fast computation for numerical calculations because the transformation can be performed by just a double FFT and an interpolation.

As rotational transformation is useful for wave optics, especially for digital holography, its formulation and usefulness were verified by demonstrating that images in tilted planes can be clearly reconstructed from the wave field captured by phase-shifting lensless Fourier digital holography.
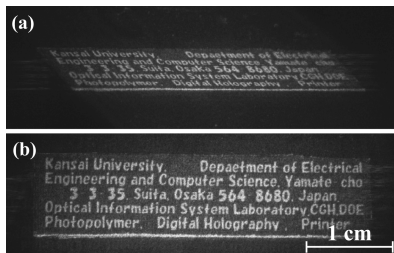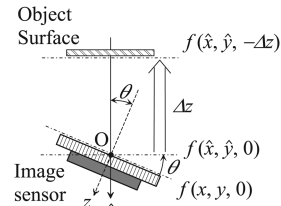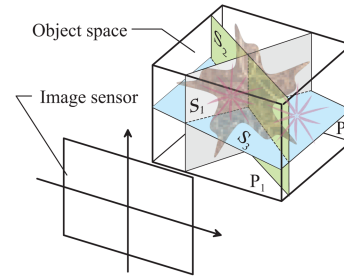
Fig. 10. Amplitude images (a) $|f'(x, y, -z_R)|$ in the parallel plane and (b) $|\hat{f}(\hat{x}, \hat{y}, 0)|$ in the tilted plane reconstructed by using rotational transformation for two-axis rotation. The planar object is rotated at −60° around the x axis prior to rotation at 30° around the y axis.

References

1. T. Tommasi and B. Bianco, "Computer-generated holograms of tilted planes by a spatial frequency approach," J. Opt. Soc. Am. A **10**, 299–305 (1993).
2. D. Leseberg, "Computer-generated three-dimensional image holograms," Appl. Opt. **31**, 223–229 (1992).
3. N. Delen and B. Hooker, "Free-space beam propagation between arbitrarily oriented planes based on full diffraction theory: a fast Fourier transform approach," J. Opt. Soc. Am. A **15**, 857–867 (1998).
4. L. Yu, Y. An, and L. Cai, "Numerical reconstruction of digital holography with changed viewing angles," J. Electron. Imaging **13**, 814–818 (2004).
5. K. Matsushima, H. Schimmel, and F. Wyrowski, "Fast calculation method for optical diffraction on tilted planes by use of the angular spectrum of plane waves," J. Opt. Soc. Am. A **20**, 1755–1762 (2003).
6. K. Matsushima, "Computer-generated holograms for three-dimensional surface objects with shade and texture," Appl. Opt. **44**, 4607–4614 (2005).
7. K. Matsushima, "Exact hidden-surface removal in digitally synthetic full-parallax holograms," Proc. SPIE **5742**, 25–32 (2005).

8. S. De Nicola, A. Finizio, G. Pierattini, P. Ferraro, and D. Alfieri, "Angular spectrum method with correction of anamorphism for numerical reconstruction of digital holograms on tilted planes," Opt. Express **13**, 9935–9940 (2005).

9. S. De Nicola, P. Ferraro, A. Finizio, and G. Pierattini, "Correct-image reconstruction in the presence of severe anamorphism by means of digital holography," Opt. Lett. **26**, 974–976 (2001).

10. J. W. Goodman, *Introduction to Fourier Optics*, 2nd ed. (McGraw-Hill, 1996), chap. 3.10.

11. J. T. Sheridan and R. Patten, "Holographic interferometry and the fractional fourier transformation," Opt. Lett. **25**, 448–450 (2000).

12. T. Nakatsuji and K. Matsushima, "Free-viewpoint images captured using phase-shifting synthetic aperture digital holography," Appl. Opt. **47** (2008), to be published.

13. I. Yamaguchi and T. Zhang, "Phase-shifting digital holography," Opt. Lett. **22**, 1268–1270 (1997).